Sixth International Symposium on Turbulence and Shear Flow Phenomena
Seoul, Korea, 22-24 June 2009

ANISOTROPY PROPERTIES OF ROTATING SHEARED TURBULENCE

Frank G. Jacobitz
Mechanical Engineering Program, University of San Diego
5998 Alcalá Park, San Diego, California 92110, USA,
jacobitz@sandiego.edu

Wouter J. T. Bos
LMFA, UMR CNRS 5509, Ecole Centrale de Lyon - Université Claude Bernard Lyon 1 - INSA de Lyon,
69134 Ecully Cedex, France,
wouter.bos@ec-lyon.fr

Kai Schneider
M2P2-CNRS & CMI, Université de Provence,
39 rue Joliot-Curie, 13453 Marseille Cedex 13, France,
kschneid@cmi.univ-mrs.fr

Marie Farge
LMD-IPSL-CNRS, Ecole Normale Supérieure,
24 rue Lhomond, 75231 Paris Cedex 5, France,
farge@lmd.ens.fr

ABSTRACT

The anisotropy properties of homogeneous turbulence with mean shear and system rotation are studied using both conventional and wavelet-based anisotropy measures. The study is based on a series of nine direct numerical simulations in which the rotation ratio f/S of Coriolis parameter to shear rate is varied. The presence of rotation stabilizes the flow, except for a narrow range of rotation ratios $0 < f/S < 1$. The main mechanism for the destabilization is an increased turbulence production due to increased anisotropy. This anisotropy at large and small scales is quantified by applying conventional measures, such as the Reynolds stress and the dissipation rate anisotropy tensors, respectively. Recently introduced directional wavelet based measures are also applied and compared with the classical ones.

INTRODUCTION

Rotation and shear are ubiquitous features of many geophysical flows and engineering applications (e.g. Miesch, 2005). The prototypical flow studied here has constant vertical shear $S = \partial U_1/\partial x_2$. System rotation with constant Coriolis parameter $f = 2\Omega$ is considered and the rotation axis is perpendicular to the plane of shear. It is therefore directed into the spanwise direction x_3 and parallel or anti-parallel to the mean flow vorticity. The Cartesian coordinates $\mathbf{x} = (x_1, x_2, x_3)$ refer to the streamwise, vertical, and spanwise directions, respectively. A schematic of the mean flow configuration is shown in figure 1.

In previous studies (Bradshaw, 1969; Tritton, 1992) the effect of rotation was found to be destabilizing in the anti-parallel configuration with $0 < f/S < 1$ and stabilizing otherwise. Comprehensive investigations of this flow include the work by Salhi and Cambon (1997), Brethouwer (2005) and Jacobitz et al. (2008). Linear theory has been used by Salhi (2002) to investigate the similarities of rotation and stratification in such flows. An overview on homogeneous turbulence dynamics including shear flows can be found in a recent monograph by Sagaut and Cambon (2008).

The aim of this study is an investigation of the anisotropy properties of homogeneous turbulence with shear and rotation. In particular, well established anisotropy measures, such as the Reynolds stress and dissipation rate anisotropy tensors, are compared to wavelet-based measures of anisotropy recently introduced by Bos et al. (2007). Directional energies and the corresponding spatial fluctuations can be quantified using the orthogonal wavelet decomposition. The scale dependent directional flatness allows furthermore to quantify the intermittency of the flows. Therewith the influence of the rotation rate on the directional statistics and the flow intermittency can be analyzed.

DIRECT NUMERICAL SIMULATIONS

The direct numerical simulations performed here are based on the continuity equation for an incompressible fluid and the unsteady three-dimensional Navier-Stokes equation. In the direct numerical approach, all dynamically important scales of the velocity field are resolved. The equations are solved in a frame of reference moving with the mean flow (Rogallo, 1981). This approach allows the application of periodic boundary conditions for the fluctuating components of the velocity field. A spectral collocation method is used for the spatial discretization and the solution is advanced in time with a fourth-order Runge-Kutta scheme. The simulations are performed on a parallel computer using a grid with $256 \times 256 \times 256$ points. The simulations analyzed in this study are identical to the ones reported in Jacobitz et al. (2008).

In the following, results of nine simulations of rotating sheared turbulence are presented. In the simulations, the ro-

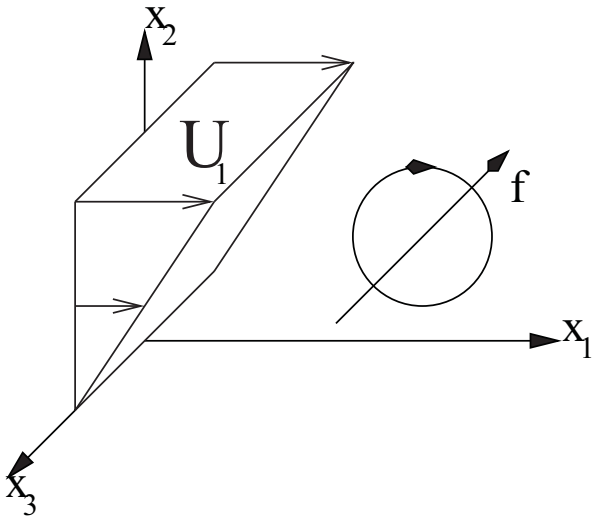

Figure 1: Schematic of the mean flow configuration with uniform vertical shear $S = \partial U_1/\partial x_2$ and rotation $f = 2\Omega$. Note that this schematic shows a parallel configuration with negative rotation ratio f/S.

tation ratio f/S was varied from -10 to 10. Negative values of f/S correspond to the parallel configuration and positive values correspond to the anti-parallel configuration. All simulations are initialized with isotropic turbulence fields. The initial Taylor microscale Reynolds number $Re_\lambda = 45$ and the initial shear number $SK/\epsilon = 2$ are matched in all cases. The Reynolds number reaches values as high as $Re_\lambda = 120$ and the shear number assumes a value of about $SK/\epsilon = 6$ in the simulations.

RESULTS

In this section, first the turbulence evolution is discussed. Then the anisotropy properties of the turbulence are characterized using well-established measures. Finally, wavelet-based measures are used to obtain further information about the anisotropy properties of homogeneous turbulence with mean shear and system rotation.

Turbulence Evolution

Figure 2 shows the evolution of the turbulent kinetic energy K for a series of simulations in which the rotation ratio f/S is varied. Due to the isotropic initial conditions, the turbulent kinetic energy first decays. The non-rotating case with $f/S = 0$ shows eventual exponential growth of K. For moderate rotation ratios, the anti-parallel case with $f/S = +0.5$ leads to strong growth of the turbulent kinetic energy, while the parallel case with $f/S = -0.5$ results in decay of K. For strong rotation ratios, however, both the anti-parallel case with $f/S = +10$ and the parallel case with $f/S = -10$ lead to strong decay of K due to the importance of linear effects. These observations are in agreement with previous results (Bradshaw, 1969; Tritton, 1992; Brethouwer, 2005).

The transport equation for the turbulent kinetic energy can be written in the following form:

$$\gamma = \frac{1}{SK}\frac{dK}{dt} = \frac{P}{SK} - \frac{\epsilon}{SK} \qquad (1)$$

Here γ is the growth rate of the turbulent kinetic energy, P/SK the normalized production rate, and ϵ/SK the normalized dissipation rate. The dependence of the turbulence

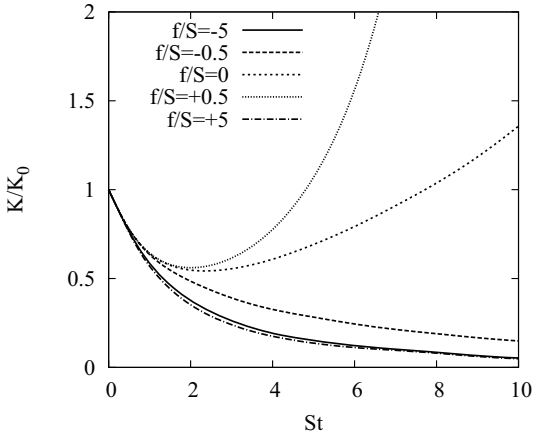

Figure 2: Evolution of the turbulent kinetic energy K in non-dimensional time St for different rotation ratios f/S.

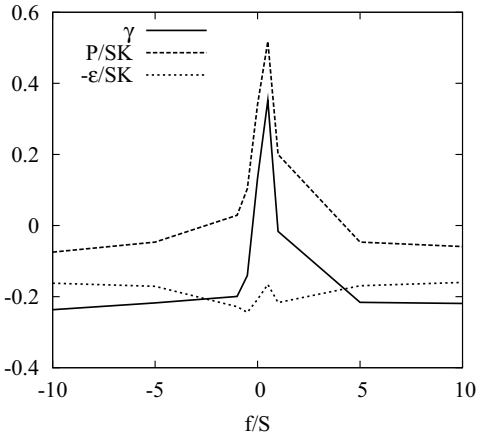

Figure 3: Dependence of the growth rate γ, normalized production P/SK, and normalized dissipation ϵ/SK on the rotation ratio f/S at non-dimensional time $St = 5$.

growth rate γ on the rotation ratio f/S is shown in figure 3 at non-dimensional time $St = 5$. Positive values of γ correspond to growth of the turbulent kinetic energy K and negative values of γ correspond to decay of K. In accordance with previous work the anti-parallel configuration with $0 < f/S < 1$ results in a destabilization of the flow, while other parameter ranges of the rotation ratio lead to a stabilization of the turbulence. Both normalized production P/SK and normalized dissipation ϵ/SK contribute to the growth rate γ. While the normalized dissipation rate remains relatively unaffected by a variation of the rotation ratio, the normalized production rate strongly increases in the anti-parallel case with $0 < f/S < 1$, resulting in the strong increase in turbulence growth.

It was found from volume visualization of vortical structures that the dependence of the growth rate γ on the rotation ratio f/S directly follows the dependence of the inclination angle α on f/S. The angle α describes the inclination of vortical structures in the vertical direction to the downstream direction. A case with strongly growing turbulent kinetic energy K is characterized by more strongly inclined vortical structures and a decaying case is characterized by a smaller inclination angle α. A more detailed discussion of the inclination angle α can be found in Jacobitz et al. (2008).

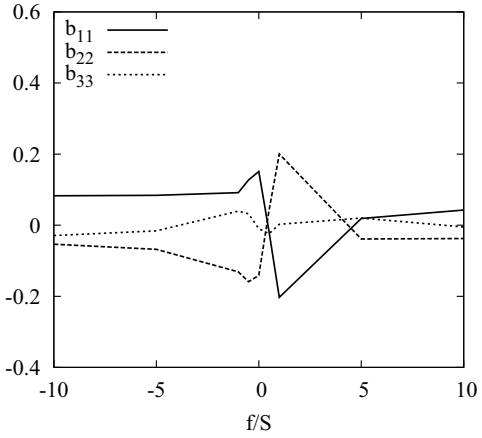

Figure 4: Dependence of the diagonal components of the Reynolds stress anisotropy tensor $b_{\alpha\beta}$ on the rotation ratio f/S at non-dimensional time $St = 5$.

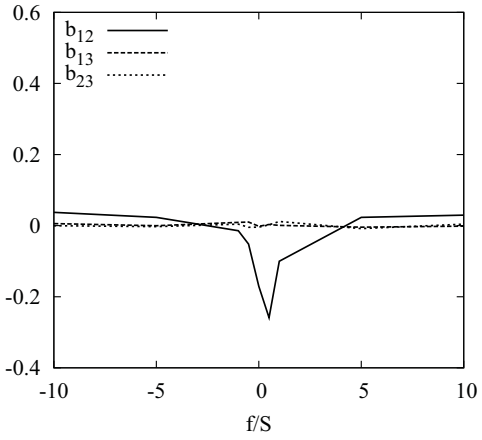

Figure 5: Dependence of the off-diagonal components of the Reynolds stress anisotropy tensor $b_{\alpha\beta}$ on the rotation ratio f/S at non-dimensional time $St = 5$.

Conventional Anisotropy Measures

Two conventional measures for the anisotropy properties of turbulent flow are computed from the direct numerical simulation data. The Reynolds stress anisotropy tensor $b_{\alpha\beta}$ is considered to describe the large scale anisotropy properties:

$$b_{\alpha\beta} = \frac{\overline{u_\alpha u_\beta}}{2K} - \frac{1}{3}\delta_{\alpha\beta} \tag{2}$$

Figure 4 shows the dependence of the diagonal components of the Reynolds shear stress anisotropy tensor $b_{\alpha\beta}$ on the rotation ratio f/S at non-dimensional time $St = 5$. The diagonal components of $b_{\alpha\beta}$ correspond to the distribution of energy on the velocity components. For most rotation ratios, an ordering $b_{11} > b_{33} > b_{22}$, or streamwise > spanwise > vertical, is observed. Only in the anti-parallel cases with $0 < f/S < 1$ this ordering is changed to $b_{22} > b_{33} > b_{11}$, or vertical > spanwise > streamwise. The off-diagonal components of $b_{\alpha\beta}$ are shown in figure 5. Due to the symmetry of the flow, the components b_{13} and b_{23} remain small. The magnitude of the component b_{12} is largest for $f/S = +0.5$, corresponding to the strongest growth of the turbulent kinetic energy K. Note that $P/SK = -2b_{12}$, relating the normalized turbulence production rate to the anisotropy features of the flow.

The dissipation rate anisotropy tensor $e_{\alpha\beta}$ is defined in a similar manner to describe the small scale anisotropy properties:

$$e_{\alpha\beta} = \frac{\nu\overline{\frac{\partial u_\alpha}{\partial x_k}\frac{\partial u_\beta}{\partial x_k}}}{2\epsilon} - \frac{1}{3}\delta_{\alpha\beta} \tag{3}$$

Figure 6 shows the dependence of the diagonal components of the dissipation rate anisotropy tensor $e_{\alpha\beta}$ on the rotation ratio f/S at non-dimensional time $St = 5$. Both the streamwise e_{11} and spanwise e_{33} components generally show a surplus, while the vertical component e_{22} shows a deficit. Only in the strongly growing case with rotation ratio $f/S = 0.5$, the ordering is altered. The off-diagonal components of $e_{\alpha\beta}$ are shown in figure 7. Again only the e_{12} component is non-zero. Overall, the components of the dissipation rate anisotropy tensor $e_{\alpha\beta}$ follow closely the components of the Reynolds stress anisotropy tensor $b_{\alpha\beta}$. The main drawback of the dissipation rate anisotropy tensor is the summation over all three gradients of velocity in each component. It is therefore not possible to capture additional directional information about this flow not already described in the Reynolds stress anisotropy tensor.

In order to gain more understanding of directional information contained in the velocity gradients, the contribution

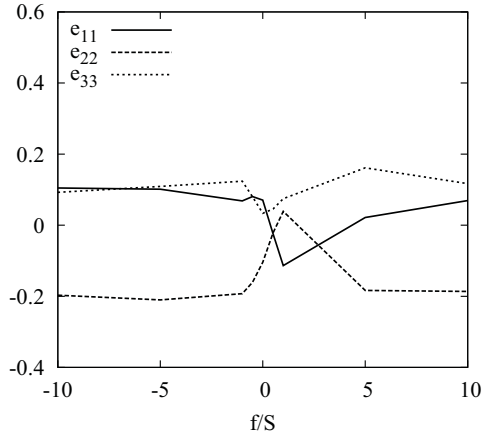

Figure 6: Dependence of the diagonal components of the dissipation rate anisotropy tensor $e_{\alpha\beta}$ on the rotation ratio f/S at non-dimensional time $St = 5$.

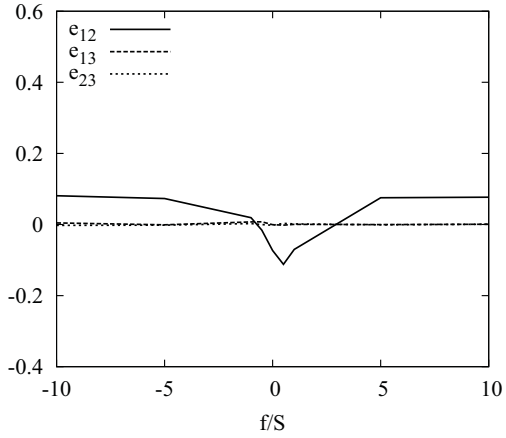

Figure 7: Dependence of the off-diagonal components of the dissipation rate anisotropy tensor $e_{\alpha\beta}$ on the rotation ratio f/S at non-dimensional time $St = 5$.

of each gradient to the overall dissipation rate is considered:

$$\epsilon_{\alpha,\beta} = \frac{\nu \overline{\frac{\partial u_\alpha}{\partial x_\beta} \frac{\partial u_\alpha}{\partial x_\beta}}}{2\epsilon} \tag{4}$$

No summation is implied over the velocity components of the spatial derivatives. The top row in figure 8 shows the dependence of $\epsilon_{\alpha,\beta}$ on the rotation ratio f/S at non-dimensional time $St = 5$. The left figure shows the three gradients of the streamwise velocity component $\epsilon_{1,\beta}$. For most values of the rotation ratio, the vertical component is the largest. It is, however, strongly reduced for the strongly growing cases with $0 < f/S < 1$ where the spanwise component becomes important. The center figure shows the gradients of the vertical velocity component $\epsilon_{2,\beta}$. Again the spanwise gradient is strongly increased for the cases with strongly growing turbulent kinetic energy. The right figure shows the gradients of the spanwise velocity component $\epsilon_{3,\beta}$. For most cases the vertical gradient shows the largest contribution, but it is reduced for the cases with strongly growing turbulent kinetic energy. In general, by magnitude large rotation ratios lead to large spanwise gradients of the velocity components. The cases with growing turbulent kinetic energy, however, are characterized by strong vertical gradients of the velocity components.

Wavelet-based Anisotropy Measures

Space–scale decomposition of the flow is obtained by applying the orthogonal wavelet transform to the velocity field. Therefore, the velocity field $\mathbf{u} = (u_1, u_2, u_3)$ at a given time instant is developed onto an orthogonal wavelet basis using Coiflet 12 wavelets (Farge, 1992). The projection of one component $u_\alpha(\mathbf{x})$ can be represented by

$$u_\alpha(\mathbf{x}) = \sum_\lambda \tilde{u}_\lambda^\alpha \, \psi_\lambda(\mathbf{x}) \tag{5}$$

with the subscript $\lambda = (j, \mathbf{i}, d)$, where j represents the scale, $\mathbf{i}$ the position and d the direction. Due to orthogonality the wavelet coefficients are given by $\tilde{u}_\lambda^\alpha = \langle u_\alpha, \psi_\lambda \rangle$, where $\langle , \rangle$ denotes the L^2-inner product. The wavelet coefficients measure the fluctuations of u_α at scale 2^{-j} and around position $\mathbf{i}/2^j$ for each of the seven possible directions d. The contribution of u_α at scale 2^{-j} and direction d is obtained by fixing j and d and summing only over $\mathbf{i}$ in equation 5 and is denoted by $u_\alpha^{j,d}$.

Parseval's identity allows to obtain directional energy contributions (Bos et al., 2007), which also depend on scale. For the directional scale dependent energy distribution of a velocity component u_α we thus obtain:

$$E_\alpha^{j,d} = \frac{1}{2} \langle u_\alpha, u_\alpha \rangle \tag{6}$$

Summing over all scales we get the directional energy of the velocity component u_α in the direction d:

$$E_\alpha^d = \sum_j E_\alpha^{j,d} \tag{7}$$

By construction we obtain the total kinetic energy as follows:

$$E = \sum_{j,d} E_\alpha^{j,d} = \sum_d E_\alpha^d \tag{8}$$

To study higher order scale dependent statistics we define the p-th order centered moments of each component u_α of the vector field $\mathbf{u}$ at scale j by its wavelet coefficients (Schneider et al. 2004):

$$M_{p,j}^\alpha = \frac{1}{7 \times 2^{3j}} \sum_{\mathbf{i}=0}^{2^j-1} \sum_{d=1}^{7} \left[\tilde{u}_\lambda^\alpha - \bar{M}_j^\alpha \right]^p \tag{9}$$

Here

$$\bar{M}_j^\alpha = \sum_{\mathbf{i}=0}^{2^j-1} \sum_{d=1}^{7} \tilde{u}_\lambda^\alpha / (7 \times 2^{3j}) \tag{10}$$

denotes the mean value at scale j. The scale dependent flatness of a velocity component u_α is defined as follows:

$$F_j^\alpha = M_{4,j}^\alpha / \left(M_{2,j}^\alpha \right)^2 \tag{11}$$

It is closely related to the standard deviation of the spectral distribution of energy, which illustrates that F_j^ℓ yields a measure for the relative spatial fluctuations of the spectral energy density (Bos et al., 2007).

Relating the scale index j with a wavenumber k_j by $k_j = k_0 2^j$ where k_0 is the centroid wavenumber, being constant for each type of wavelet ($k_0 \approx 0.77$ for the Coiflet 12 used here), the scale dependent distributions (energy, skewness or flatness) can be related to wavenumber distributions, e.g. energy spectra (Bos et al., 2007).

The bottom row in figure 8 shows directional energy components E_α^d/E for the x, y and z components. These wavelet based measures exhibit a striking similarity with the directional dissipation rate components $e_{i,j}/e$. This is due to the fact that wavelet coefficients measure fluctuations of velocity components in one of the seven possible directions and they thus can be related to velocity gradients.

The directional scale-dependent flatness of the three velocity components is plotted in figure 9. Here we focus only on two cases, one for $f/S = +0.5$ (top) which is representative for a flow with strongly growing energy, and one for $f/S = +5$ which represents the energy decaying flows. A general feature of all curves is a strong increase of the flatness with wavenumber, which reflects the flow intermittency. It can also be observed that the growth of flatness of all velocity components is the strongest in the streamwise direction, except for the case $f/S = +0.5$ where the flatness of the u_1 velocity component behaves similarly in all directions due to the strong shear production.

CONCLUSIONS

The results of nine direct numerical simulations of homogeneous turbulence with shear and rotation are evaluated for anisotropy properties of this flow. The turbulent kinetic energy was found to grow strongly in the anti-parallel configuration with $0 < f/S < 1$ and to decay otherwise. The growth is due to an increased normalized turbulence production $P/SK = -2b_{12}$ that is directly related to the only non-zero off-diagonal component of the Reynolds stress anisotropy tensor. It was also observed that the growth rate of the turbulence is related to the inclination angle of vortical structures to the downstream direction (Jacobitz et al., 2008).

The directional energy of the flow, based on orthogonal wavelets, allows to give an alternative description of the anisotropy of the flow. Wavelets, like structure functions, are sensitive to velocity differences in the different directions. This allows to characterize longitudinal and transversal anisotropy. Furthermore, orthogonal wavelets

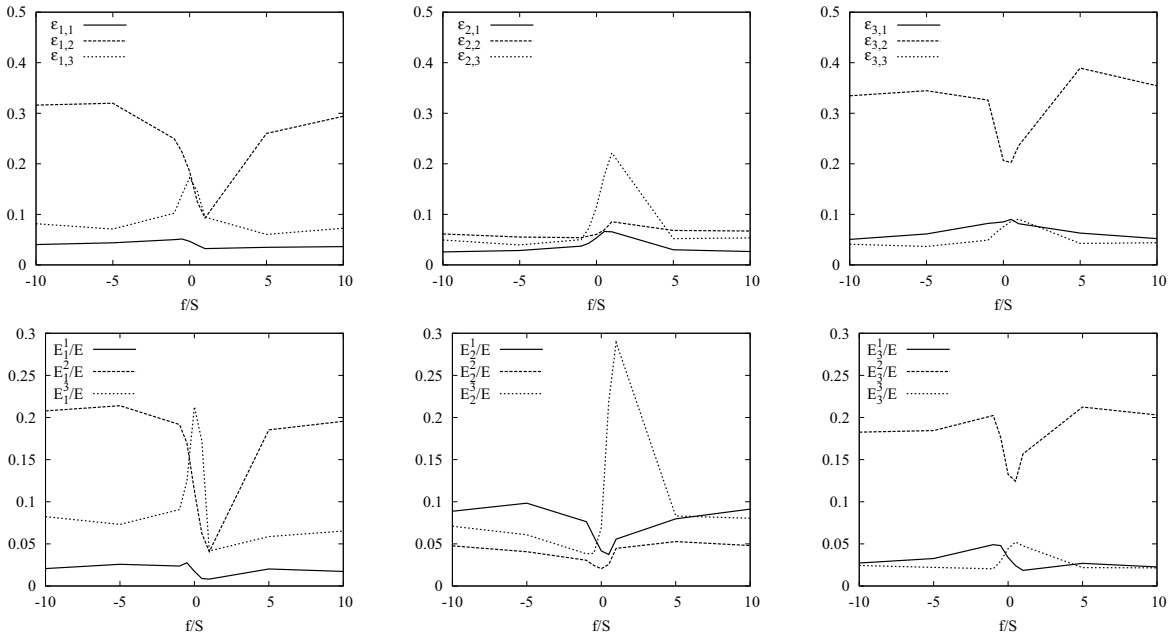

Figure 8: Dependence of the dissipation rate component $\epsilon_{\alpha,\beta}$ for $\beta = 1, 2$ and 3 (top) and directional energy component E^d_α/E for $d = 1, 2$ and 3 (bottom) on the rotation ratio f/S at non-dimensional time $St = 5$. The x_1 component (left), x_2 component (center), and x_3 component (right) are shown.

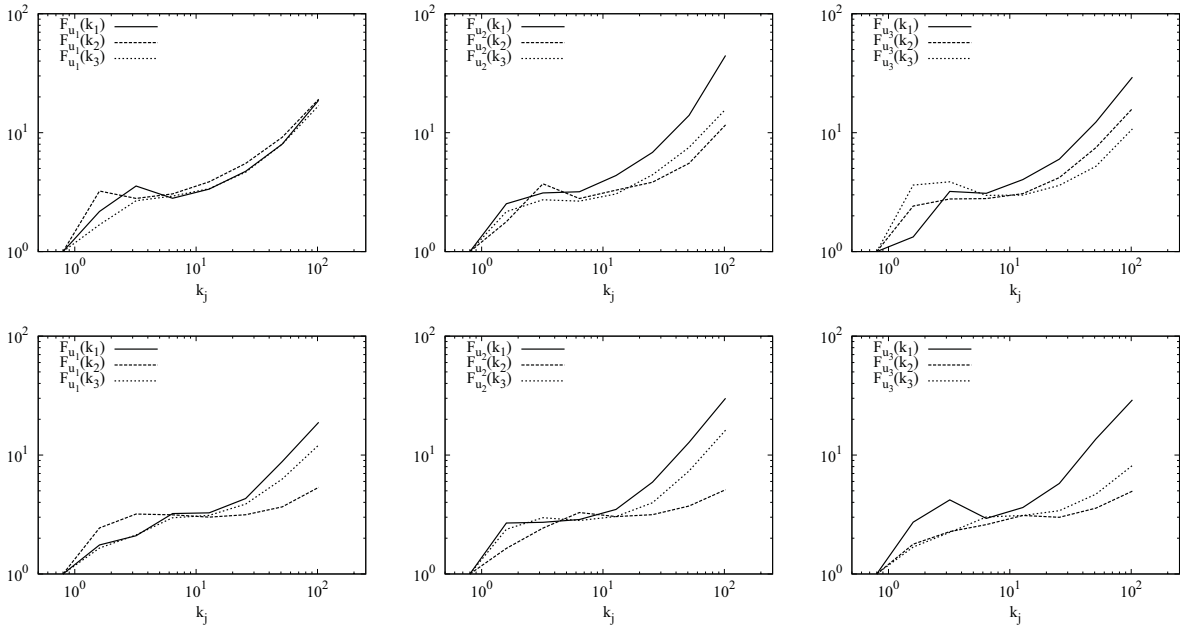

Figure 9: Directional scale-dependent flatness for $f/S = +0.5$ (upper row) and $f/S = +5$ (lower row). The u_1 component (left), u_2 component (center), and u_3 component (right) are shown.

have the advantage that, by construction, the energy contained in the different direction sums up to the total energy, unlike structure functions or one-dimensional spectra. For the strongly growing case with $f/S = +0.5$ the spanwise differences of vertical velocity contain most of the energy, followed by the spanwise differences of downstream velocity. For the strongly decaying case with $f/S = +5$, however, the vertical differences of spanwise and downstream velocities contain most of the energy, while vertical velocity is strongly reduced. Wavelet based directional energy measures agree with conventional measures and allow furthermore to quantify the flow intermittency in different directions.

ACKNOWLEDGMENTS

FGJ acknowledges support from the Ecole Centrale Marseille and an International Opportunity Grant from the University of San Diego. WB, MF and KS acknowledge financial support from the ANR, project M2TFP and KS thanks the Institut Carnot STAR for partial financial support.

REFERENCES

Bos, W. J. T., Liechtenstein, L., and Schneider, K., 2007, "Small scale intermittency in anisotropic turbulence", *Phys. Rev. E*, Vol. 76, 046310.

Bradshaw, P., 1969, "The analogy between streamline curvature and buoyancy in turbulent shear flow", *J. Fluid Mech.*, Vol. 36, pp. 177–191.

Brethouwer, G., 2005, "The effect of rotation on rapidly sheared homogeneous turbulence and passive scalar transport. Linear theory and direct numerical simulations", *J. Fluid Mech.*, Vol. 542, pp. 305–342.

Farge, M., 1992, "Wavelet transforms and their applications to turbulence", *Annu. Rev. Fluid Mech.*, Vol. 24, pp. 395–458.

Jacobitz, F. G., Liechtenstein, L., Schneider, K., and Farge, M., 2008, "On the structure and dynamics of sheared and rotating turbulence: Direct numerical simulation and wavelet-based coherent vortex extraction", *Phys. Fluids*, Vol. 20.

Miesch, M. S., 2005, "Large-scale dynamics of the convection zone and tachocline", *Living Rev. Solar Phys.*, Vol. 2, 1.

Rogallo, R. S., 1981, "Numerical experiments in homogeneous turbulence", *Technical Report TM 81315*, NASA, Moffett Field, CA.

Sagaut, P., and Cambon C., 2008, *Homogeneous Turbulence Dynamics*, Cambridge University Press.

Salhi, A., and Cambon, C., 1997 "An analysis of rotating shear flow using linear theory and DNS and LES results", *J. Fluid Mech.*, Vol. 347, pp. 171–195.

Salhi, A., 2002, "Similarities between rotation and stratification effects on homogeneous shear flow", *Theoret. Comp. Fluid Dyn.*, Vol. 15, pp. 339–358.

Schneider, K., Farge, M., and Kevlahan, N., 2004, "Spatial intermittency in two-dimensional turbulence: a wavelet approach", *Woods Hole Mathematics, Perspectives in Mathematics and Physics, Vol. 34* (Eds. N. Tongring and R.C. Penner), World Scientific, 302–328.

Tritton, D. J., 1992, "Stabilization and destabilization of turbulent shear flow in a rotating fluid", *J. Fluid Mech.*, Vol. 241, pp. 503–523.